

# Reduction of NO by CO over nanoscale $\text{LaCo}_{1-x}\text{Cu}_x\text{O}_3$ and $\text{LaMn}_{1-x}\text{Cu}_x\text{O}_3$ perovskites

Runduo Zhang<sup>a</sup>, Adrian Villanueva<sup>a</sup>, Houshang Alamdari<sup>b</sup>, Serge Kaliaguine<sup>a,\*</sup>

<sup>a</sup> Department of Chemical Engineering, Laval University, Ste Foy (QC), Canada G1K 7P4

<sup>b</sup> Nanox Inc., 4975 rue Rideau, Local 100, Que., Canada G2E 5H5

Received 23 February 2006; received in revised form 24 April 2006; accepted 1 May 2006

Available online 16 June 2006

## Abstract

Nanoscale perovskites with nominal formula of  $\text{La}(\text{Co}, \text{Mn})_{1-x}\text{Cu}_x\text{O}_3$  were generated by a novel method designated as reactive grinding and characterized by  $\text{N}_2$  adsorption, X-ray diffraction (XRD), temperature programmed desorption (TPD) of  $\text{O}_2$ , NO, and CO, temperature programmed surface reduction (TPSR) of NO under CO/He flow. Activity tests of NO + CO reaction for those materials were also carried out in this study. A better catalytic performance (93%  $\text{N}_2$  yield and 91% CO conversion at 500 °C) was found over  $\text{LaCoO}_3$  compared to  $\text{LaMnO}_3$  (76%  $\text{N}_2$  yield and 76% CO conversion at 500 °C), with a reaction atmosphere of 3000 ppm NO and 3000 ppm CO in helium at a space velocity of 50,000  $\text{h}^{-1}$ . The catalytic activity in NO + CO reaction for  $\text{LaCoO}_3$  can be considerably improved via 20% Cu substitution, leading to a 97%  $\text{N}_2$  yield and nearly complete CO conversion at 450 °C. This improvement was ascribed to the ease of generation of anion vacancies after Cu incorporation, which plays a crucial role in NO adsorption and dissociation. In addition, the enhancement in lattice oxygen mobility of Cu substituted perovskites promotes the CO oxidation and anion vacancy recovery giving another clue for this improvement.  $\text{N}_2\text{O}$  decomposition (68%  $\text{N}_2$  yield at 500 °C) is much easier than NO decomposition (below 5% at  $T < 500$  °C). Both NO and  $\text{N}_2\text{O}$  conversions are significantly improved by the reducing agent. A mechanism was proposed with dissociation of chemisorbed NO forming  $\text{N}_2$  and/or  $\text{N}_2\text{O}$ , and oxidized perovskite surface, with continuous reduction by CO with the production of  $\text{CO}_2$ .  $\text{O}_2$  has a strongly detrimental effect leading to the easy consumption of the reducing agent via CO oxidation.

© 2006 Elsevier B.V. All rights reserved.

**Keywords:** NO reduction; Carbon monoxide; Reactive grinding; High surface area; Perovskite

## 1. Introduction

NO and CO, two main pollutants in exhaust gases from gas-line engines can cause serious environmental problems such as photochemical smog, acid rain and respiratory diseases. It would be an ideal way to simultaneously eliminate those pollutants via catalytic reduction of NO using CO as a reducing agent. Three-way-catalysts (TWC), mainly composed of platinum and rhodium metal deposited on a  $\text{CeO}_2$ - $\gamma$ - $\text{Al}_2\text{O}_3$  coating, were widely studied for this interconversion between NO and CO [1]. Efforts for the replacement of supported noble metals are however deemed necessary, because of the drawbacks of noble metals in practical application, including high cost, volatilization and sintering at high temperature [2].

Perovskites oxides having the general formula of  $\text{ABO}_3$ , where B usually designates a transition metal cation surrounded by six oxygens in octahedral coordination, and A is a cation of rare-earth metal coordinated by 12 oxygens, have been considered as promising alternatives to precious metals acting as effective TWC due to their low cost, high thermal stability, and diverse physicochemical properties. Some perovskites were shown to be active in CO oxidation as early as in 1952 [3]. Since Libby showed their potential application for purification of exhaust gases, perovskites have been recognized as valuable catalysts for the catalytic reduction of NO by CO [4].

Among the perovskite-type oxides, lanthanum cobaltite and lanthanum manganite have attracted more attention for this kind of study due to their special oxygen nonstoichiometries [5]. Their properties can be further modified by the partial substitution of A- or B-site cations. Much research has been done concerning the A-site substitution and its effect in catalytic activities toward NO reduction by CO was considered to be related with the defective structure and valence alternation after substi-

\* Corresponding author. Tel.: +1 418 656 2708; fax: +1 418 656 3810.  
E-mail address: [kaliaguine@gch.ulaval.ca](mailto:kaliaguine@gch.ulaval.ca) (S. Kaliaguine).

tution [6–10]. However, much less work was reported about the effect of B-site substitution on the physicochemical properties of perovskites as well as their catalytic performances for the interconversion of NO and CO [11].

Copper containing catalysts are of special interest as they are active in a wide range of reactions for transformation of nitrogen oxides, as reviewed by Centi and Perathoner [12]. Highly dispersed  $\text{Cu}^{2+}$  was generally regarded as an active site for NO reduction [13–17]. A good performance may therefore be expected by incorporation of fully isolated copper cations into the B-site of the perovskite structure.

The application of perovskites has to some extent been limited by their low specific surface areas resulting from the rather high temperature at which they are usually generated (700–800 °C) [18]. Some perovskite preparation methods including microemulsion [19], citrate complexation [20], coprecipitation [21], sol–gel process [22], spray–drying [23], freeze–drying [24], and flame–hydrolysis [25], were attempted in order to improve their surface areas. We have shown recently that a large variety of perovskites can be synthesized at essentially room temperature by reactive grinding which allowed to achieve a specific surface area in excess of 100 m<sup>2</sup>/g [26–28].

The aim of the present work is to investigate the influence of Cu substitution on the physicochemical properties of  $\text{LaCo}_{1-x}\text{Cu}_x\text{O}_3$  and  $\text{LaMn}_{1-x}\text{Cu}_x\text{O}_3$  ( $x=0, 0.1, \text{ and } 0.2$ ) prepared by reactive grinding, in order to clarify the relation between perovskite properties and their catalytic behaviors in the reaction between NO and CO. Attempt was also made to propose an overall mechanism for the catalytic action of perovskites in this reaction.

## 2. Experimental

Two series of  $\text{LaCo}_{1-x}\text{Cu}_x\text{O}_3$  and  $\text{LaMn}_{1-x}\text{Cu}_x\text{O}_3$  solid solutions were prepared by reactive grinding. Powders of  $\text{La}_2\text{O}_3$  (Alfa, 99.99%), CuO (Aldrich, 99.98%), and  $\text{Co}_3\text{O}_4$  (Baker & Adamson, 97.49%) or  $\text{Mn}_3\text{O}_4$  (Baker & Adamson, 98.22%) in desired proportions were milled under high energy, using a SPEX grinder rotated at 1100 rpm, equipped with tempered steel vial and three tempered steel balls. The  $\text{La}_2\text{O}_3$  powder was preliminarily calcined at 600 °C for 24 h in order to eliminate any trace of lanthanum hydroxide. ZnO was added as a leachable additive during grinding to further enhance the specific surface areas of the products.

The specific surface area and pore size distribution of mixed oxides were determined by  $\text{N}_2$  adsorption at liquid nitrogen temperature from the linear part of the BET curve ( $P/P_0=0.01\text{--}0.10$ ) and from the desorption branch of  $\text{N}_2$  isotherms using the Barrett–Joyner–Halenda (BJH) formula, respectively. Samples of about 200 mg were evacuated at 300 °C for 6 h prior to the adsorption/desorption experiments.

The elemental analysis of the end products (Co, Mn, Cu) and the residual impurities (Zn, Fe) was made by atomic absorption spectroscopy (AAS) (1100B, Perkin-Elmer) after dissolution of samples in a mixture of 10% HCl solution and concentrated HF. The analysis of La was accomplished by inductively coupled plasma (ICP) spectrometry (Optima 4300DV, Perkin-Elmer).

XRD patterns of the solids were recorded using a diffractometer (D5000, Siemens) with monochromatized Cu K $\alpha$  radiation ( $\lambda=1.5406 \text{ \AA}$ ) in the range  $10^\circ < 2\theta < 80^\circ$  at a scan rate of 0.05° every 2.4 s. The crystal phases were confirmed according to JCPDS reference while the crystallite sizes were calculated on the basis of Scherrer equation after Warren's correction.

Temperature programmed desorption (TPD) of  $\text{O}_2$ , NO, and CO were performed in a fixed-bed reactor with the effluent gases monitored using a quadrupole mass spectrometer (MS) (UTI 100). Prior to TPD of  $\text{O}_2$ , NO, and CO experiments, 50 mg samples were treated with the various atmospheres of 10%  $\text{O}_2$  or 3000 ppm NO or 3000 ppm CO balanced by helium, respectively, with a total flow rate of 20 cm<sup>3</sup>/min at 500 °C for 1 h, then cooled down to room temperature under the same atmosphere, and subsequently flushed by 20 cm<sup>3</sup>/min He for 40 min to remove the physisorbed molecules. Finally, the reactor temperature was raised up to 500 °C (800 °C for  $\text{O}_2$ -TPD) at a constant heating rate of 10 °C/min.  $\text{O}_2$ , NO, CO and  $\text{CO}_2$  desorbed during TPD experiments were simultaneously monitored by MS with the mass numbers of 32, 30, 28 and 44, respectively.

Temperature programmed surface reduction (TPSR) of NO under CO/He flow was performed with the same sample pretreatment as that during TPD of NO experiment. The thermodesorption was however performed under 1000 ppm CO/He instead of He. The MS signals recorded in this case were those of mass numbers 14, 32, 30, 28 and 44. The gaseous response obtained by MS was calibrated using standard gas mixtures.

The catalyst activity tests of  $\text{LaMn}_{1-x}\text{Cu}_x\text{O}_3$  and  $\text{LaCo}_{1-x}\text{Cu}_x\text{O}_3$  for the NO + CO reaction were carried out in a plug flow reactor at atmospheric pressure. A mixture of 3000 ppm NO and 3000 ppm CO at a total rate of 60 ml/min, corresponding to a GHSV of 50,000 h<sup>-1</sup> was passed through the catalyst bed containing about 100 mg catalyst. In addition, the gas compositions of 3000 ppm  $\text{N}_2\text{O}$  + 3000 ppm CO or 3000 ppm NO or 3000 ppm  $\text{N}_2\text{O}$  or 3000 ppm CO or 3000 ppm CO + 1500 ppm  $\text{O}_2$  were also adopted for the reactions of  $\text{N}_2\text{O}$  + CO, NO or  $\text{N}_2\text{O}$  decomposition, CO oxidation by perovskite or oxygen, respectively, over  $\text{LaCo}_{0.8}\text{Cu}_{0.2}\text{O}_3$  under the same space velocity. The system was heated externally in a tubular furnace, regulated by an Omega controller in the temperature region of 100–500 °C via a thermocouple in contact with the catalyst bed. NO and  $\text{NO}_2$  in effluent were analyzed by chemiluminescence NO/ $\text{NO}_2$ / $\text{NO}_x$  analyzer (Model 200AH, API Inc.).  $\text{N}_2\text{O}$  and CO gases were monitored using a FT-IR gas analyzer (FTLA 2000, ABB Inc.).  $\text{N}_2$  was detected using a gas chromatograph (GC) (Hewlett Packard 5890) equipped with a thermal conductivity detector (TCD) and columns of molecular 13X (45–60 mesh, 2.4 m) combined with Silicone OV-101 (100–120 mesh, 0.6 m). Calibration was done using standard gases containing known concentrations of the components.

## 3. Results

### 3.1. Physicochemical properties

The chemical composition of the prepared oxides was determined by AAS and ICP showing values close to the nominal

Table 1  
Properties of  $\text{LaCo}_{1-x}\text{Cu}_x\text{O}_3$  and  $\text{LaMn}_{1-x}\text{Cu}_x\text{O}_3$  mixed oxides after calcination at  $500^\circ\text{C}$  for 5 h

Sample	Chemical composition <sup>a</sup>	Specific surface area ( $\text{m}^2/\text{g}$ )	Pore diameter (nm)	Crystallite size (nm)	Crystal phase	Perovskite structure
$\text{LaCoO}_3$	$\text{La}_{1.05}\text{Co}_{1.0}\text{O}_{3\pm\delta}$	29.2	18.1	11.8	$\text{LaCoO}_3/\text{La}_2\text{O}_2\text{CO}_3^b/\text{Co}_3\text{O}_4^b$	Rhombohedral
$\text{LaCo}_{0.9}\text{Cu}_{0.1}\text{O}_3$	$\text{La}_{1.0}\text{Co}_{0.86}\text{Cu}_{0.14}\text{O}_{3\pm\delta}$	23.8	15.6	10.8	$\text{LaCoO}_3/\text{Co}_3\text{O}_4^b$	Rhombohedral
$\text{LaCo}_{0.8}\text{Cu}_{0.2}\text{O}_3$	$\text{La}_{0.97}\text{Co}_{0.76}\text{Cu}_{0.24}\text{O}_{3\pm\delta}$	22.4	14.7	9.2	$\text{LaCoO}_3/\text{Co}_3\text{O}_4^b$	Rhombohedral
$\text{LaMnO}_3$	$\text{La}_{0.98}\text{Mn}_{1.0}\text{O}_{3\pm\delta}$	40.6	10.8	11.3	$\text{LaMnO}_3/\text{La}_2\text{O}_2\text{CO}_3^b$	Rhombohedral
$\text{LaMn}_{0.9}\text{Cu}_{0.1}\text{O}_3$	$\text{La}_{0.97}\text{Mn}_{0.91}\text{Cu}_{0.09}\text{O}_{3\pm\delta}$	40.7	12.4	13.0	$\text{LaMnO}_3$	Rhombohedral
$\text{LaMn}_{0.8}\text{Cu}_{0.2}\text{O}_3$	$\text{La}_{1.1}\text{Mn}_{0.78}\text{Cu}_{0.22}\text{O}_{3\pm\delta}$	42.6	10.8	14.4	$\text{LaMnO}_3/\text{La}_2\text{O}_2\text{CO}_3^b/\text{CuO}^b$	Rhombohedral

<sup>a</sup> Fe and Zn can be detected as contaminants with a combined wt.% less than 2% of the total weight of prepared  $\text{La}(\text{Co}, \text{Mn})_{1-x}\text{Cu}_x\text{O}_3$  samples.

<sup>b</sup> Minor phases.

formulation (Table 1). The BET surface areas and pore diameters of these materials synthesized by reactive grinding after calcination at  $500^\circ\text{C}$  for 5 h are also reported in Table 1, representing specific surface areas of  $20\text{--}30\text{ m}^2/\text{g}$  for cobalt lanthanates and approximately  $40\text{ m}^2/\text{g}$  for manganese lanthanates even after calcination. Higher surface areas and smaller pore diameters were observed for  $\text{LaMn}_{1-x}\text{Cu}_x\text{O}_3$  oxides compared to  $\text{LaCo}_{1-x}\text{Cu}_x\text{O}_3$  ones.

The crystallite phase identification of solid solutions was accomplished by means of XRD with the results being given in Table 1. The comparison of experimental spectra with JCPDS charts indicates that all Co-containing samples are essentially rhombohedral perovskite-type mixed oxides (JCPDS card 48-0123). Other minor phases, such as  $\text{Co}_3\text{O}_4$  (JCPDS card 42-1467) in the case of all Co-based catalysts, and  $\text{La}_2\text{O}_2\text{CO}_3$  (JCPDS card 37-0804) in the case of  $\text{LaCoO}_3$ , were detected in addition to the major  $\text{ABO}_3$  perovskite phase. The XRD lines of Mn-containing samples also mainly correspond to the rhombohedral perovskite structure and with the formula  $\text{LaMnO}_{3.15}$  for the unsubstituted lanthanum manganite (JCPDS card 50-0298). Minor phases, such as  $\text{CuO}$  (JCPDS card 80-1268) in the case of  $\text{LaMn}_{0.8}\text{Cu}_{0.2}\text{O}_3$  and  $\text{La}_2\text{O}_2\text{CO}_3$  (JCPDS card 37-0804) in the case of  $\text{LaMnO}_3$  and  $\text{LaMn}_{0.8}\text{Cu}_{0.2}\text{O}_3$ , were detected as crystalline impurities. The crystallite sizes of all prepared perovskites were subsequently calculated by Scherrer equation and listed in Table 1 with values (9–15 nm) close to those of their pore diameters (10–18 nm) determined from  $\text{N}_2$  desorption isotherms. It is thus inferred that the present samples had a somewhat porous structure formed via clustering of individual primary particles in agreement with reference [29].

### 3.2. Temperature programmed desorption of oxygen ( $\text{O}_2$ -TPD)

Due to the distinct oxygen nonstoichiometry of lanthanum cobaltites (oxygen deficiency) and lanthanum manganites (oxygen excess), the oxygen desorption behaviors over the above two series of perovskite-type oxides were widely studied and well documented to correlate nonstoichiometric oxygen of perovskites with their catalytic characteristics in redox reactions [30]. The  $\text{O}_2$  species adsorbed over Co- and Mn-based perovskites generated by reactive grinding were thus investigated via  $\text{O}_2$ -TPD experiments as depicted in Fig. 1. The amounts of  $\text{O}_2$  released were calculated after deconvolution of the  $\text{O}_2$

desorption curves using Lorentzian peak shape and reported in Table 2.

Two kinds of desorption peaks are present in the  $\text{O}_2$ -TPD spectrum of  $\text{LaCoO}_3$ : the broad one appearing in the range of  $150\text{--}720^\circ\text{C}$  was ascribed to  $\alpha\text{-O}_2$  desorption and related to molecular  $\text{O}_2$  adsorbed on oxygen vacancies [27]. The latter peak with a maximum at  $797^\circ\text{C}$  was designated as  $\beta\text{-O}_2$  desorption and attributed to the liberation of  $\text{O}_2$  from the lattice [27]. With the partial substitution of Co by Cu, the desorption of  $\alpha\text{-O}_2$  is significantly enhanced in proportion to the substitution degree. This result indicates that more oxygen vacancies can be generated over Co-based perovskites after Cu incorporation into B-site of lattice likely due to a positive charge compensation in agreement with the previous report [30]. Additionally, the  $\beta\text{-O}_2$  desorption of Cu-substituted lanthanum cobaltites can take place at relatively lower temperature (with the former ones at about  $765^\circ\text{C}$  and the latter ones at about  $795^\circ\text{C}$ ) with respect to  $\text{LaCoO}_3$  suggesting the mobility of lattice  $\text{O}_2$  was also improved via Cu substitution.

A minor  $\alpha\text{-O}_2$  peak at  $T < 450^\circ\text{C}$  was found in the  $\text{O}_2$ -TPD profile for  $\text{LaMnO}_3$  associated with a slight enhancement in its intensity upon increasing Cu content. A following intense desorption with a maximum at  $608^\circ\text{C}$  was observed over lanthanum manganite, showing a drop in its intensity after Cu substitution. The introduction of Cu ions in  $\text{LaMnO}_3$  perovskite lattice

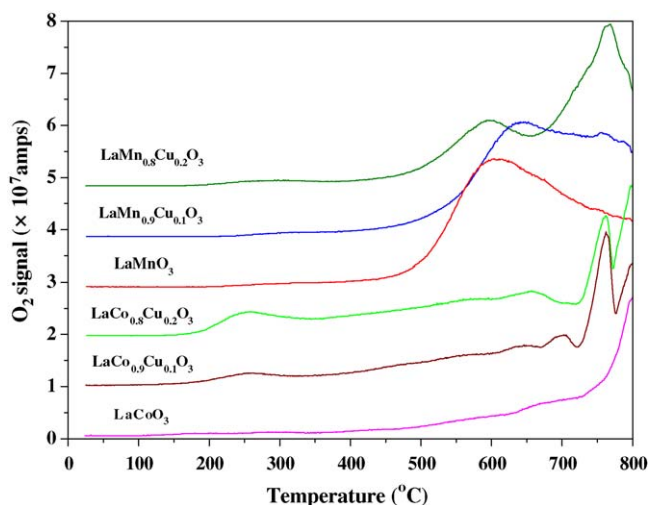


Fig. 1. TPD of  $\text{O}_2$  profiles of  $\text{LaCo}_{1-x}\text{Cu}_x\text{O}_3$  and  $\text{LaMn}_{1-x}\text{Cu}_x\text{O}_3$  perovskites [15,16].

Table 2

Amounts of O<sub>2</sub> desorbed from LaCo<sub>1-x</sub>Cu<sub>x</sub>O<sub>3</sub> and LaMn<sub>1-x</sub>Cu<sub>x</sub>O<sub>3</sub> perovskites during O<sub>2</sub>-TPD experiments [15,16]

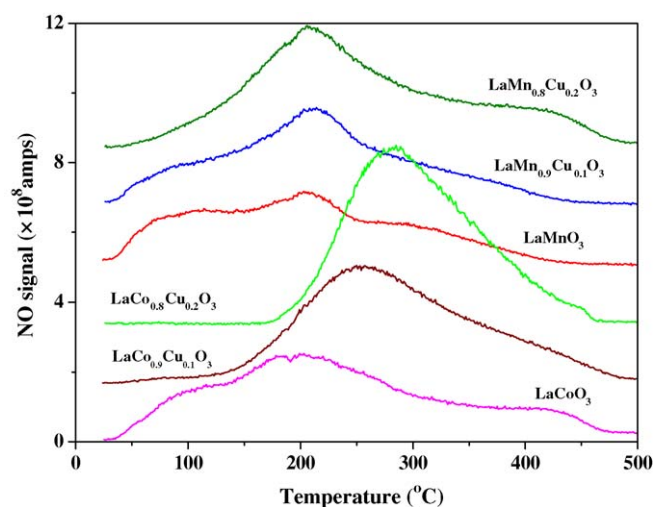
Sample	Amount of oxygen desorbed <sup>a</sup>			Number of monolayers desorbed <sup>b</sup>		
	$\alpha$ -O <sub>2</sub> ( $\mu\text{mol g}^{-1}$ )	Excess oxygen ( $\mu\text{mol g}^{-1}$ ) <sup>c</sup>	$\beta$ -O <sub>2</sub> ( $\mu\text{mol g}^{-1}$ )	$\alpha$ -O <sub>2</sub>	Excess oxygen	$\beta$ -O <sub>2</sub>
LaCoO <sub>3</sub>	133.2 (<720 °C)	–	112.4 (720–800 °C)	1.14	–	0.96
LaCo <sub>0.9</sub> Cu <sub>0.1</sub> O <sub>3</sub>	252.2 (<720 °C)	–	163.6 (720–800 °C)	2.65	–	1.72
LaCo <sub>0.8</sub> Cu <sub>0.2</sub> O <sub>3</sub>	285.6 (<720 °C)	–	171.6 (720–800 °C)	3.19	–	1.91
LaMnO <sub>3</sub>	16.8 (324 °C)	316.7 <sup>c</sup> (609 °C)	–	0.10	1.95	–
LaMn <sub>0.9</sub> Cu <sub>0.1</sub> O <sub>3</sub>	22.6 (323 °C)	189.3 <sup>c</sup> (646 °C)	155.7 (760 °C)	0.14	1.16	0.96
LaMn <sub>0.8</sub> Cu <sub>0.2</sub> O <sub>3</sub>	40.1 (301 °C)	106.8 <sup>c</sup> (599 °C)	196.1 (763 °C)	0.23	0.62	1.15

<sup>a</sup> Calculated by deconvolution of the O<sub>2</sub> desorption curves.<sup>b</sup> Calculated with 4  $\mu\text{mol m}^{-2}$  of oxygen per monolayer (Ref. [27]).<sup>c</sup> The excess oxygen calculated according to the second O<sub>2</sub> desorption peak under the region of 400–650 °C.

was reported to suppress its overstoichiometric (excess) oxygen [5]. This peak is therefore associated with the desorption of overstoichiometric oxygen of lanthanum manganite. This overstoichiometric oxygen desorbed in parent LaMnO<sub>3</sub> was quantified and found to be consistent with the formula of LaMnO<sub>3.15</sub> determined by XRD. This can be interpreted as another evidence supporting the ascription of overstoichiometric oxygen in O<sub>2</sub>-TPD profiles. The  $\beta$ -O<sub>2</sub> desorption from Mn-based perovskites are believed to correspond to those peaks appearing at temperatures above 700 °C. It seems that the lattice O<sub>2</sub> mobility of lanthanum manganite is improved again via substituting B-site ion by Cu according to the results reported in Table 2. The promotion in the mobility of lattice oxygen of lanthanum cobaltite and manganite after Cu B-site substitution had also been observed in our early H<sub>2</sub>-TPR studies [15,16]. The trace amounts of  $\alpha$ -O<sub>2</sub> desorbing from LaMn<sub>0.8</sub>Cu<sub>0.2</sub>O<sub>3</sub> suggest that Cu substitution has indeed produced oxygen vacancies, which can coexist with the overstoichiometric oxygen in the lattice. However, this  $\alpha$ -O<sub>2</sub> desorption is severely suppressed compared to LaCo<sub>1-x</sub>Cu<sub>x</sub>O<sub>3</sub> which is associated with the presence of overstoichiometric oxygen.

### 3.3. Temperature programmed desorption of NO (NO-TPD)

The MS signal of NO ( $m/e = 30$ ) [along with O<sub>2</sub> ( $m/e = 32$ )] as function of desorption temperature was recorded during NO-TPD under He flow for LaCo<sub>1-x</sub>Cu<sub>x</sub>O<sub>3</sub> and LaMn<sub>1-x</sub>Cu<sub>x</sub>O<sub>3</sub> perovskites as reported in Fig. 2. The amount of NO desorbed from perovskites was further calculated based on deconvolution of these curves (Table 3). A broad NO desorption centered

Fig. 2. MS signal of NO during TPD of NO of LaCo<sub>1-x</sub>Cu<sub>x</sub>O<sub>3</sub> and LaMn<sub>1-x</sub>Cu<sub>x</sub>O<sub>3</sub> perovskites.

at 200 °C with one minor shoulder at 90 °C and another at 388 °C was observed in the TPD of NO profiles for LaCoO<sub>3</sub>. Upon Cu substitution the low temperature peak is entirely suppressed, the 200 °C one is substantially increased and shifted to higher temperature so that it interferes with the minor high temperature one. Similar NO desorption features were found for LaMnO<sub>3</sub> after NO adsorption, representing three superimposed desorption peaks with maxima at 100, 202 and 311 °C, respectively. With the increase of Cu percentage in LaMn<sub>1-x</sub>Cu<sub>x</sub>O<sub>3</sub>, the low temperature peak is totally suppressed whereas the high temperature one grows and is slightly shifted towards higher

Table 3

Amounts of NO desorbed from LaCo<sub>1-x</sub>Cu<sub>x</sub>O<sub>3</sub> and LaMn<sub>1-x</sub>Cu<sub>x</sub>O<sub>3</sub> perovskites during NO-TPD experiments

	Physisorbed NO <sup>a</sup> ( $\mu\text{mol g}^{-1}$ )	Nitrosyl species <sup>a</sup> ( $\mu\text{mol g}^{-1}$ )	Nitrate species <sup>a</sup> ( $\mu\text{mol g}^{-1}$ )	Chemisorbed NO	
				( $\mu\text{mol g}^{-1}$ )	( $\mu\text{mol m}^{-2}$ ) <sup>b</sup>
LaCoO <sub>3</sub>	2.4 (90 °C)	27.6 (201 °C)	9.4 (388 °C)	37.0	1.27
LaCo <sub>0.9</sub> Cu <sub>0.1</sub> O <sub>3</sub>	–	39.9 (255 °C)	–	39.9	1.68
LaCo <sub>0.8</sub> Cu <sub>0.2</sub> O <sub>3</sub>	–	45.7 (283 °C)	–	45.7	2.04
LaMnO <sub>3</sub>	8.8 (100 °C)	15.9 (202 °C)	5.8 (311 °C)	21.7	0.53
LaMn <sub>0.9</sub> Cu <sub>0.1</sub> O <sub>3</sub>	5.7 (106 °C)	23.5 (210 °C)	6.0 (323 °C)	29.5	0.72
LaMn <sub>0.8</sub> Cu <sub>0.2</sub> O <sub>3</sub>	–	31.5 (209 °C)	9.7 (361 °C)	41.2	0.96

<sup>a</sup> Calculated by deconvolution of NO desorption curves.<sup>b</sup> Calculated with the specific surface areas in Table 1.

Table 4  
Amounts of CO and CO<sub>2</sub> desorbed from LaCo<sub>1-x</sub>Cu<sub>x</sub>O<sub>3</sub> and LaMn<sub>1-x</sub>Cu<sub>x</sub>O<sub>3</sub> perovskites during CO-TPD experiments

Sample	CO		CO <sub>2</sub>		Total carbonaceous species
	T (°C)	Amount (μmol g <sup>-1</sup> )	T (°C)	Amount (μmol g <sup>-1</sup> )	Amount (μmol g <sup>-1</sup> )
LaCoO <sub>3</sub>	>200	26.6	>200	116.4	143.0
LaCo <sub>0.9</sub> Cu <sub>0.1</sub> O <sub>3</sub>	>200	22.5	>150	166.4	188.9
LaCo <sub>0.8</sub> Cu <sub>0.2</sub> O <sub>3</sub>	>200	18.2	>150	195.0	213.2
LaMnO <sub>3</sub>	>250	40.5	>200	66.7	107.2
LaMn <sub>0.9</sub> Cu <sub>0.1</sub> O <sub>3</sub>	>250	56.9	>200	95.3	152.2
LaMn <sub>0.8</sub> Cu <sub>0.2</sub> O <sub>3</sub>	>250	70.5	>200	104.3	174.8

temperature. Small O<sub>2</sub> desorptions parallel with only the high-temperature NO shoulder peaks were observed during NO-TPD studies (not shown).

### 3.4. Temperature programmed desorption of CO (CO-TPD)

The desorption of CO ( $m/e=28$ ) and CO<sub>2</sub> ( $m/e=44$ ) was monitored by MS during the CO-TPD experiments for Co- and Mn-based samples. A quantitative analysis of the various carbonaceous gases desorbed from perovskites is summarized in Table 4. Both CO and CO<sub>2</sub> desorptions were observed indicating that the oxidation of CO into CO<sub>2</sub> occurs over those lanthanum perovskites during CO-TPD experiments, while Cu substitution leads to more CO<sub>2</sub> desorption over lanthanates suggesting a promotion in CO oxidation by means of copper incorporation. Simultaneously, it was observed that the amount of total carbonaceous species (CO + CO<sub>2</sub>) desorbed from perovskites also increased after Cu substitution, suggesting that copper incorporation can also facilitate the generation of adsorption sites for CO or CO<sub>2</sub>. Higher carbonaceous species was found over cobaltites with respect to manganites under the same Cu substitution percentage.

### 3.5. Temperature programmed surface reduction of NO (NO-TPSR) under CO/He

Fig. 3 represents the TPSR of adsorbed NO under 1000 ppm CO/He flow over LaCo<sub>0.8</sub>Cu<sub>0.2</sub>O<sub>3</sub>. The amounts of desorbed NO and generated N<sub>2</sub> were quantified according to the deconvolution of their MS traces. The oxygen signal detected by MS ( $m/e=32$ ) rapidly diminishes at 100–300 °C simultaneously with a consumption of CO, while a recovery of this O<sub>2</sub> signal takes place at  $T>300$  °C. At temperatures lower than 180 °C, a NO desorption peak (15.6 μmol g<sup>-1</sup>) was observed in Fig. 3 whereas it is absent in the NO desorption curve in Fig. 2. The NO desorption peak (45.7 μmol g<sup>-1</sup>) centered at 283 °C and its minor shoulder for LaCo<sub>0.8</sub>Cu<sub>0.2</sub>O<sub>3</sub> in Fig. 2 is essentially suppressed into 3.9 μmol g<sup>-1</sup> (in Fig. 3), indicating that the corresponding adsorbed NO species has reacted with CO but that the product of reaction is not desorbed over the temperature range of this experiment. Some N<sub>2</sub> desorption (3.5 μmol g<sup>-1</sup>) with a maximum at approximately 150 °C was indeed observed but not in amounts comparable with the content of a desorbed NO reported for the same sample in Fig. 2. The appearance of CO<sub>2</sub> coincides with the disappearance of CO.

### 3.6. Activity tests

A blank test was performed under 60 ml/min of 3000 ppm CO and 3000 ppm NO balanced by helium in an empty reactor (not shown). No significant NO conversion (<2%) and CO conversion (<5%) were observed up to 500 °C. Hence, the conversions generated from homogenous reaction in the absence of catalyst are essentially negligible under usual reaction conditions. Temperature dependencies of N<sub>2</sub> yields over Co- and Mn-based perovskites are shown in Fig. 4a. Among the six tested samples, the worst conversion to N<sub>2</sub> is obtained in the case of LaMnO<sub>3</sub> with a progressive increase up to 76% at 500 °C. A higher N<sub>2</sub> yield with a maximum of 93% at 500 °C was observed over LaCoO<sub>3</sub> with respect to LaMnO<sub>3</sub>. An obvious enhancement in N<sub>2</sub> yields is realized by Cu partial substitution for the two series of perovskites resulting in an approximate order of LaCo<sub>0.8</sub>Cu<sub>0.2</sub>O<sub>3</sub> > LaCo<sub>0.9</sub>Cu<sub>0.1</sub>O<sub>3</sub> > LaMn<sub>0.8</sub>Cu<sub>0.2</sub>O<sub>3</sub> > LaMn<sub>0.9</sub>Cu<sub>0.1</sub>O<sub>3</sub>. N<sub>2</sub>O is detectable in the effluent with maxima in the range of 270–330 °C depending on the solid composition as illustrated in Fig. 4b. More significant N<sub>2</sub>O production and CO conversion were found over LaCoO<sub>3</sub> compared to those obtained over LaMnO<sub>3</sub> (see Fig. 4b and c). The N<sub>2</sub>O production and CO conversion obtained over lanthanum cobaltite and lanthanum manganite can be improved via Cu substitution. In general,

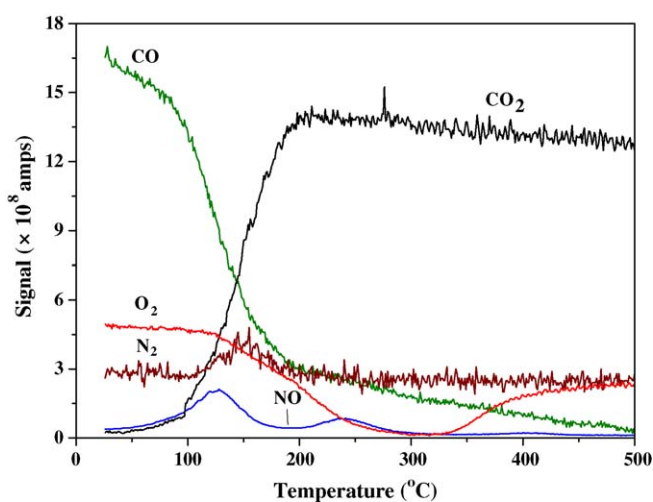


Fig. 3. MS signals during TPSR of NO under CO/He flow of LaCo<sub>0.8</sub>Cu<sub>0.2</sub>O<sub>3</sub>, conditions: flow rate = 20 ml/min, 3000 ppm NO, 1000 ppm CO, balanced by He.

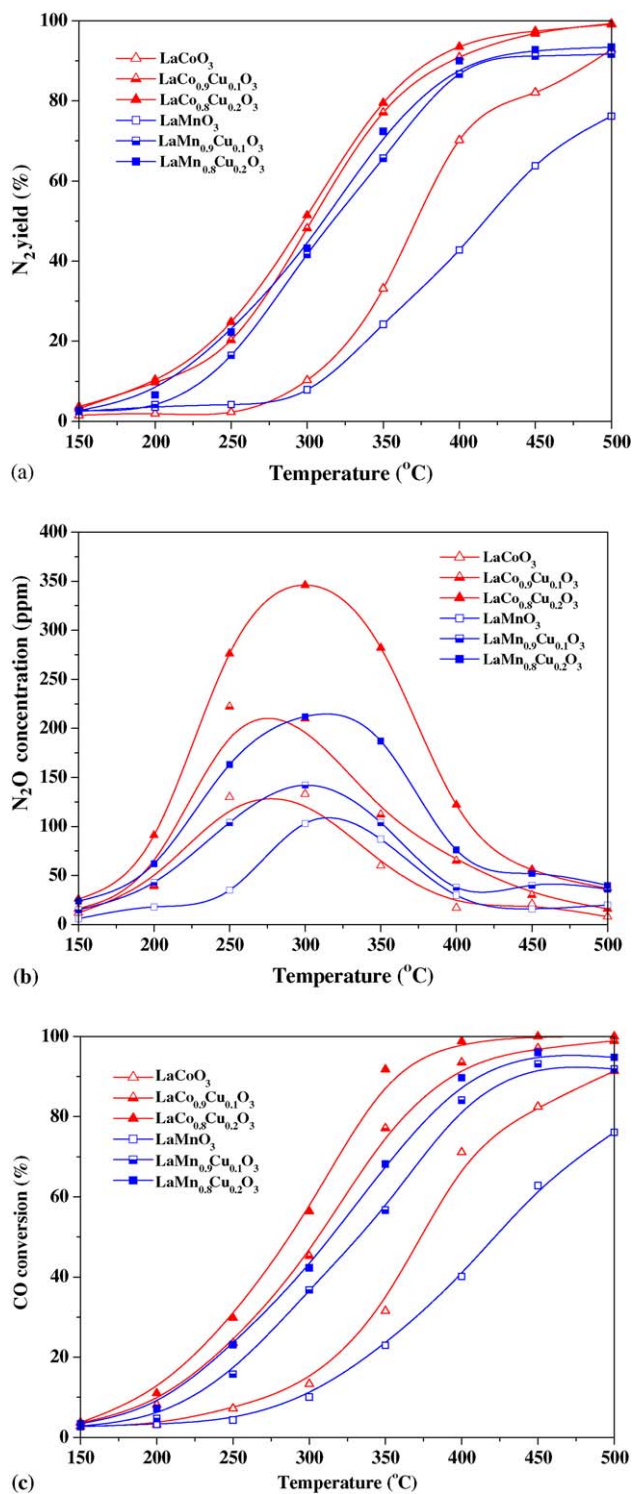


Fig. 4. (a) N<sub>2</sub> yield in CO + NO reaction over LaCo<sub>1-x</sub>Cu<sub>x</sub>O<sub>3</sub> and LaMn<sub>1-x</sub>Cu<sub>x</sub>O<sub>3</sub> perovskites, conditions: GHSV = 50,000 h<sup>-1</sup>, 3000 ppm NO, 3000 ppm CO, balanced by He. (b) N<sub>2</sub>O concentration in CO + NO reaction over LaCo<sub>1-x</sub>Cu<sub>x</sub>O<sub>3</sub> and LaMn<sub>1-x</sub>Cu<sub>x</sub>O<sub>3</sub> perovskites, conditions: GHSV = 50,000 h<sup>-1</sup>, 3000 ppm NO, 3000 ppm CO, balanced by He. (c) CO conversion in CO + NO reaction over LaCo<sub>1-x</sub>Cu<sub>x</sub>O<sub>3</sub> and LaMn<sub>1-x</sub>Cu<sub>x</sub>O<sub>3</sub> perovskites, conditions: GHSV = 50,000 h<sup>-1</sup>, 3000 ppm NO, 3000 ppm CO, balanced by He.

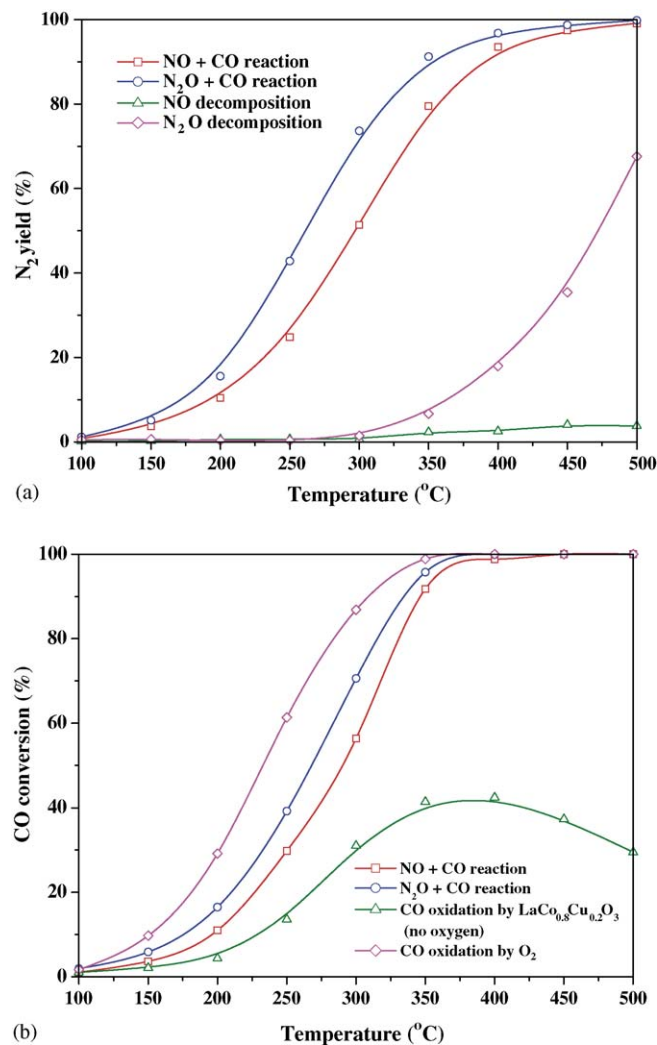


Fig. 5. (a) N<sub>2</sub> yield in various reactions over LaCo<sub>0.8</sub>Cu<sub>0.2</sub>O<sub>3</sub>. Conditions: GHSV = 50,000 h<sup>-1</sup>, 3000 ppm NO, 3000 ppm N<sub>2</sub>O, 3000 ppm CO, balanced by He. (b) CO conversion in various reactions over LaCo<sub>0.8</sub>Cu<sub>0.2</sub>O<sub>3</sub>. Conditions: GHSV = 50,000 h<sup>-1</sup>, 3000 ppm NO, 3000 ppm N<sub>2</sub>O, 3000 ppm CO, 1500 ppm O<sub>2</sub>, balanced by He.

the best performance is achieved over LaCo<sub>0.8</sub>Cu<sub>0.2</sub>O<sub>3</sub> with 94% N<sub>2</sub> yield and 99% CO conversion even at 400 °C. No obvious NO<sub>2</sub> formation was detected during activity tests of the prepared perovskites under the atmosphere of 3000 ppm NO and 3000 ppm CO.

For the best performing LaCo<sub>0.8</sub>Cu<sub>0.2</sub>O<sub>3</sub>, N<sub>2</sub> yields in the reactions of NO + CO, N<sub>2</sub>O + CO, NO decomposition and N<sub>2</sub>O decomposition were investigated and the results are shown in Fig. 5a with the objective of better understanding the NO and CO transformation in the catalytic process. In the absence of reducing agent, a little NO decomposition (<5%) occurs at 350–500 °C. N<sub>2</sub>O decomposition is much easier than NO decomposition starting at 300 °C and achieving a N<sub>2</sub>O conversion of 68% at 500 °C, possibly related to the easy cleavage of N–O bond in N<sub>2</sub>O. Nevertheless, it is noticed that N<sub>2</sub>O decomposition does not take place at *T* < 300 °C. The transformation of nitrogen oxides (NO and N<sub>2</sub>O) into N<sub>2</sub> is significantly improved

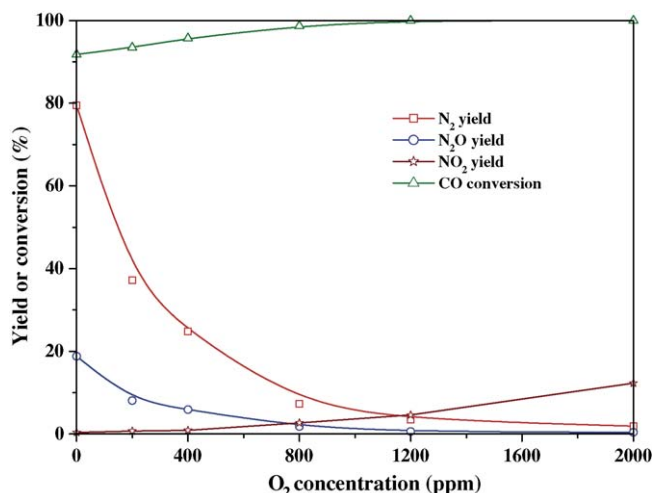


Fig. 6. Effect of O<sub>2</sub> feed concentration on catalytic performance in CO+NO reaction over LaCo<sub>0.8</sub>Cu<sub>0.2</sub>O<sub>3</sub>, conditions: GHSV = 50,000 h<sup>-1</sup>, T = 350 °C, 3000 ppm NO, 3000 ppm CO, 0–2000 ppm O<sub>2</sub>, balanced by He.

by the CO reducing agent, resulting in N<sub>2</sub> yields of 51% in NO + CO reaction and 74% in N<sub>2</sub>O + CO reaction at 300 °C and almost reaching 100% in both reactions at 500 °C. The better N<sub>2</sub> yield in N<sub>2</sub>O reduction by CO is ascribed to the easier molecular activation of N<sub>2</sub>O compared to NO.

CO conversions in reactions of NO + CO, N<sub>2</sub>O + CO, CO oxidation by perovskite (no oxygen), CO + O<sub>2</sub> over LaCo<sub>0.8</sub>Cu<sub>0.2</sub>O<sub>3</sub> are compared in Fig. 5b. CO oxidation can still carry on with a maximum conversion of 42% at 400 °C in the absence of O<sub>2</sub>, which is likely realized by consuming α-oxygen from the perovskite surface. With the consumption of adsorbed O<sub>2</sub> species by CO oxidation, a decline in CO oxidation occurs. Simultaneously, the fast desorption of O<sub>2</sub> species at relatively higher temperature, confirmed by O<sub>2</sub>-TPD (Fig. 1) and TPSR (Fig. 3) studies, also leads to this diminution in CO oxidation. Nitrogen oxides (NO and N<sub>2</sub>O) promote the CO oxidation up to 56 and 71% at 300 °C, respectively. N<sub>2</sub>O is again more active than NO to donate its oxygen atom and oxidize CO. Gaseous oxygen with the same atomic O concentration as 3000 ppm NO or N<sub>2</sub>O leads to the highest CO oxidation achieving a value of 87% even at 300 °C. The above results suggest an order of the efficiency in oxygen utilization for CO oxidation as: oxygen molecule (O<sub>2</sub>) or α-oxygen > oxygen atom (O) in NO or N<sub>2</sub>O > lattice oxygen (O<sup>2-</sup>) or β-oxygen.

The effect of O<sub>2</sub> feed concentration on catalytic performance of LaCo<sub>0.8</sub>Cu<sub>0.2</sub>O<sub>3</sub> in the NO + CO reaction at 350 °C was investigated with the results shown in Fig. 6. It was observed that the N<sub>2</sub> yield (80%) and N<sub>2</sub>O yield (19%) during NO catalytic reduction in the absence of O<sub>2</sub> decrease rapidly accompanied with the increasing O<sub>2</sub> feed concentration. 1200 ppm O<sub>2</sub> in feed is sufficient to lead to a total inhibition in N<sub>2</sub> yield resulting in a value below 5%. In contrast, the CO conversion and NO<sub>2</sub> yield are further improved by gaseous O<sub>2</sub> reaching the values of 100 and 12% at 2000 ppm O<sub>2</sub>, respectively.

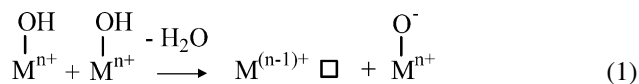
## 4. Discussion

### 4.1. O<sub>2</sub>-TPD study

A broad plateau-like α-O<sub>2</sub> desorption was observed between 200 and 720 °C over the LaCoO<sub>3</sub> perovskite. The intensity of this α-O<sub>2</sub> desorption is enhanced by Cu substitution because of a positive charge deficiency after substitution of Co<sup>3+</sup> by Cu<sup>2+</sup> compensated by oxygen vacancies [27]. This α-O<sub>2</sub> desorption was ascribed to O<sub>2</sub> adsorbed on anion vacancies, which can be readily removed at relatively low temperature. Rather poor α-O<sub>2</sub> coverage of LaMnO<sub>3</sub> after O<sub>2</sub> adsorption was found with respect to LaCoO<sub>3</sub> although its coverage can be slightly enhanced by Cu substitution, indicating a low density of anion vacancies over lanthanum manganites.

According to our previous work [27], the following process was proposed to occur during calcination of Co- or Mn-based perovskite:

- (1) Transient generation of anion vacancy during calcination of fresh sample, which seems more pronounced in the Cu substituted lanthanum cobaltites or manganites.

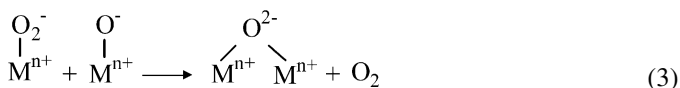


(where M=Co or Mn or Cu; n=2 or 3 or 4; □ stands for anion vacancy).

- (2) Instantaneous formation of α-O<sub>2</sub> by adsorbing O<sub>2</sub> at anion vacancy.



The two reactions (3) and (4) are proposed for the α-O<sub>2</sub> desorption process:



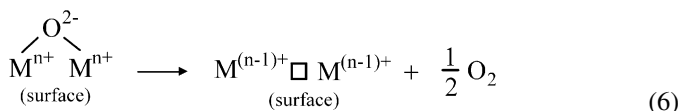
A significant desorption of overstoichiometric oxygen (excess O<sub>2</sub>) at 450–650 °C was observed over LaMnO<sub>3</sub> during O<sub>2</sub>-TPD experiments, whose intensity was suppressed by increasing Cu substitution. This may be formulated as:



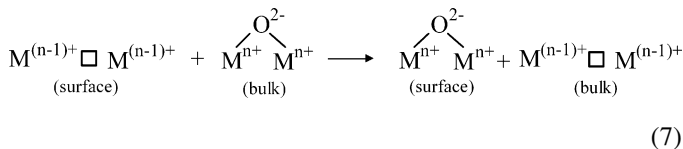
In Eq. (5) the excess oxygen charge is compensated by cation vacancies (noted here as (□)) following the suggestions of van Roosmalen et al. [31].

The β-oxygens in the surface lattice of two series of perovskites can only be desorbed at high temperature (T > 700 °C)

leading to the B-site ion reduction and anion vacancy generation.



$\beta$ -O<sub>2</sub> desorption is maintained via the diffusion of lattice oxygen from the bulk to the surface:



This  $\beta$ -oxygen desorption is promoted by Cu substitution as indicated by the results of O<sub>2</sub>-TPD experiments (Fig. 1) in accordance with the conclusion that Cu incorporation enhanced the mobility of lattice O according to our earlier studies of the reducibilities of LaCo<sub>1-x</sub>Cu<sub>x</sub>O<sub>3</sub> [15] and LaMn<sub>1-x</sub>Cu<sub>x</sub>O<sub>3</sub> [16] by H<sub>2</sub>-TPR.

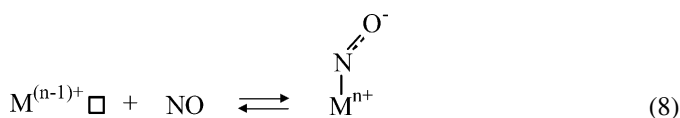
#### 4.2. NO-TPD study

The formation of (mono-, di-) nitrosyl and (monodentate, bidentate, bridging) nitrate species over LaCoO<sub>3</sub> [8,32], LaMnO<sub>3</sub> [32], Cu/ZSM-5 [33] and Cu/MCM-41 [14] after NO adsorption was mentioned in the literature. In this study, the adsorbed N-containing species formed over prepared LaCo<sub>1-x</sub>Cu<sub>x</sub>O<sub>3</sub> and LaMn<sub>1-x</sub>Cu<sub>x</sub>O<sub>3</sub> perovskites during NO adsorption were investigated by means of monitoring the NO desorption traces (*m/e* = 30) in the effluents by MS (Fig. 2). The amounts of the various NO species desorbed were quantified as listed in Table 3. It was observed that broad NO desorption peaks occur at approximately 200–280 °C with minor shoulders at their rising and falling branches, respectively, during NO-TPD experiments for Co- and Mn-based perovskites. Centi and Perathoner [12] concluded that the thermal stability of adsorbed species increased with increasing oxidation state of nitrogen in N-containing adspecies according to transient catalytic experiments over Cu/ZSM-5. In our previous TPD of NO + O<sub>2</sub> studies over Co-, Mn-based perovskites, NO peaks appearing at similar temperatures as those in NO-TPD experiments (apart from a minor desorption at medium temperature and an intense one at high temperature) were also found and ascribed to the desorptions of physisorbed NO, nitrosyl species and nitrate species depending on their thermal stability [15,16]. The NO peaks obtained at low (90–110 °C), medium (200–210 °C), and high (310–390 °C) temperatures in the present NO-TPD analyses were thus correlated to physisorbed NO, nitrosyl and nitrate species.

O<sub>2</sub> desorption simultaneous with minor NO desorption peaks occurring at 388 °C for LaCoO<sub>3</sub> and 311 °C for LaMnO<sub>3</sub> (not shown) gives another clue for the ascription of these peaks to nitrate species. This is in agreement with the report that the desorption of NO<sub>3</sub><sup>-</sup> species would appear as a NO desorption peak at high temperature (*T* > 300 °C) associated with O<sub>2</sub> desorption [15–17,34,35]. The intensity of the nitrate species peak increases

upon Cu substitution in the case of lanthanum manganites. The NO desorption peak related to nitrate species is however totally immersed in the broad peak attributed to nitrosyl species due to the shift of the latter to higher temperature at increasing Cu content in lanthanum cobaltites. It is noticeable that only minor nitrate species was formed over perovskites after NO adsorption, showing rather as a shoulder than a peak compared to nitrosyl species.

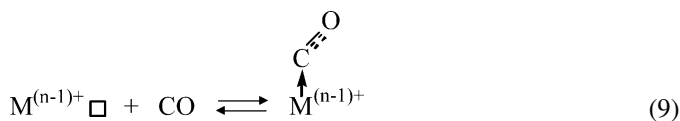
The intensities of nitrosyl species for unsubstituted LaCoO<sub>3</sub> and LaMnO<sub>3</sub> is enhanced upon Cu substitution. Based on the fact that more oxygen vacancies can be formed via substituting trivalent cation (Co<sup>3+</sup>, Mn<sup>3+</sup>) by bivalent cation (Cu<sup>2+</sup>) (due to a positive charge deficiency confirmed by O<sub>2</sub>-TPD experiments, see Fig. 1), this intense NO desorption peak related to nitrosyl species is likely formed by NO adsorption on anion vacancies as verified by Shin et al via FT-IR study [36]. The NO chemisorption as a negatively charged form (NO<sup>-</sup>) was thought to be the first important step for NO + CO reaction [37] because of the back-donation which occurs through antibonding orbitals, determines a weakening of the N–O bond when the net electron transfer is from metal to NO. The formation of nitrosyl species is formulated on the basis of the above discussion.



By taking into account the different specific surface areas of Co-based and Mn-based perovskites, the total amount of chemically adsorbed NO species was also quantified in terms of  $\mu\text{mol m}^{-2}$ . This showed more than twice more desorption occurring over Co-based samples compared to the corresponding Mn-based samples at the same Cu contents (see Table 3). This tendency coincides with the abundance of anion vacancies over lanthanum cobaltites compared to lanthanum manganites.

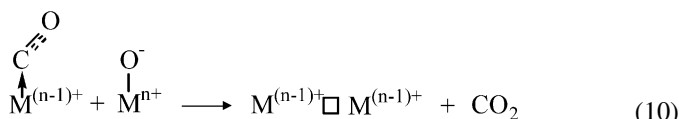
#### 4.3. CO-TPD study

According to the reports of Tascón et al., the inhibiting effect of NO on subsequent CO adsorption is larger than the inhibiting effect of CO on NO adsorption over both LaCoO<sub>3</sub> and LaMnO<sub>3</sub> [38]. It is thus speculated that CO appears to be more weakly adsorbed than NO at the same site of perovskites. The CO adsorption thus likely involves an adsorption at anion vacancies nevertheless via coordinative bond without electron transfer:

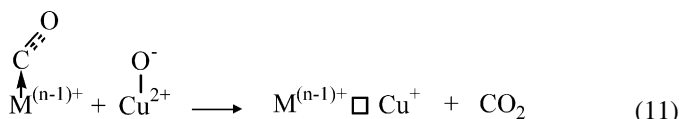


CO is oxidized into CO<sub>2</sub> over perovskites during CO-TPD experiments (Table 4) and this CO oxidation is promoted by Cu substitution leading to an enhancement in CO<sub>2</sub> desorption. It was reported that CO oxidation happens via a suprafacial catalytic process involving a surface lattice atomic oxygen (O<sup>-</sup>) [39]. The

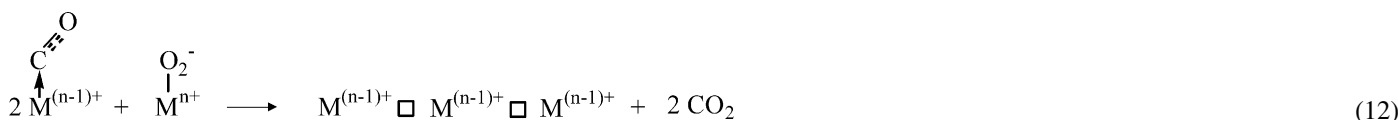
CO oxidation therefore was proposed as the following step:



Furthermore, the lower binding energy for this surface lattice oxygen favors CO oxidation [40]. The improvement of CO oxidation after Cu substitution can therefore be explained by an enhanced mobility of perovskite lattice oxygen as found in the present O<sub>2</sub>-TPD experiments and in previous H<sub>2</sub>-TPR studies [15,16].



In the presence of gaseous O<sub>2</sub>, this CO oxidation can also be accelerated by α-O<sub>2</sub> over perovskite [40] expressed as the following reaction.



#### 4.4. TPSR of NO under CO/He flow

It was observed in Fig. 3 that the NO desorption peaks related to nitrosyl and nitrate species (observed in NO-TPD profile of LaCo<sub>0.8</sub>Cu<sub>0.2</sub>O<sub>3</sub> in Fig. 2) almost vanished. Only the desorption peak appearing at low temperature, which was ascribed to physisorbed NO, is present in the NO-TPSR trace. This result suggests that both nitrosyl and nitrate species are quite active toward CO and fully consumed by this reducing agent in agreement with the previous conclusion that the chemisorbed NO plays an important role in NO + CO reaction catalyzed by perovskites [41]. Nitrate species were also proven to be highly reactive towards propene over perovskites [15–17], towards methane over Ag/Al<sub>2</sub>O<sub>3</sub> [34] and Ag-ZSM-5 [42] and resulted in a good deNO<sub>x</sub> activity at high temperature. The reactivity of this nitrate species towards CO is confirmed again in the present TPSR study. Nevertheless, the nitrate species formed over perovskites in the absence of gas phase oxygen is minor compared to nitrosyl species according to NO-TPD study. Furthermore, NO reduction is already remarkable at  $T < 300^\circ\text{C}$  (see Figs. 4a and b) whereas the nitrate species seems to be stable under this temperature range and only corresponds to high temperature activity. Nitrosyl species are therefore believed to make a most significant contribution to NO reduction by CO and their role will be emphasized in this study.

The MS signal of O<sub>2</sub> decreased progressively in the range of 100–300 °C simultaneously with the CO consumption and CO<sub>2</sub> formation due to a rapid CO oxidation (Fig. 3). Nevertheless, a recovery of O<sub>2</sub> signal was observed at  $T > 300^\circ\text{C}$ . This is likely related to a fast desorption of O<sub>2</sub> species at relatively high temperature. The O<sub>2</sub> consumption by CO to CO<sub>2</sub> oxidation is also slightly slowed down (see CO<sub>2</sub> trace in Fig. 3) possibly due to a

significant surface coverage of carbonate species, giving another explanation for this phenomenon.

N<sub>2</sub> production was also detected during this experiment implying that the reduction of nitrosyl species by CO is associated with the catalytic process.

#### 4.5. Activity test and reaction mechanism

The direct decomposition of NO would represent the most attractive solution in NO emission control, because the reaction does not require that any reactant be added to NO exhaust gas and could potentially lead to the formation of only N<sub>2</sub> and O<sub>2</sub>. In principle, the simple NO decomposition is a thermodynamically favored reaction at low temperature. However, this reaction is very slow due to the high dissociation energy of NO (153.3 kcal mol<sup>-1</sup>) and no sufficiently efficient catalysts have been discovered so far [43]. Up to now Cu-zeolites are the best catalysts with isolated Cu<sup>+</sup> ions regarded as active centres in NO decomposition [13]. Perovskites exhibit an activity better

than most of other metal oxides for this reaction, but at 500 °C they are much less active than the best copper zeolites [44–46]. That NO hardly decomposes over LaCo<sub>0.8</sub>Cu<sub>0.2</sub>O<sub>3</sub> perovskite at <500 °C was confirmed again in this work (Fig. 5a).

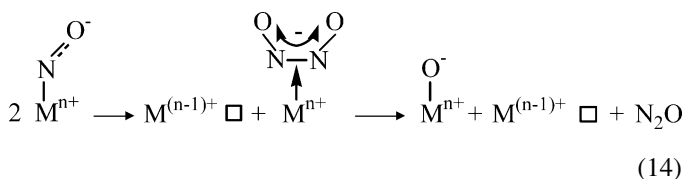
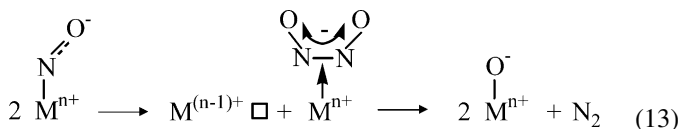
Nitrous oxide is not toxic but plays a role in ozone depletion. N<sub>2</sub>O decomposition over LaCo<sub>0.8</sub>Cu<sub>0.2</sub>O<sub>3</sub> was thereafter examined with the result in Fig. 5a showing a better activity in terms of N<sub>2</sub> yield (68% at 500 °C) than that achieved in NO decomposition (4% at 500 °C). N<sub>2</sub>O is known to have a linear structure N–N–O in which the N–N bond length is somewhat longer than that in triply bonded N<sub>2</sub> (1.09 Å) and in which the N–O distance is increased by about 0.03 Å relative to free nitric oxide with a bond order of 2.5, resulting in an easy cleavage of its N–O bond and better dissociation behavior. However, enough energy is still necessary for N–O bond breakage according to the result that N<sub>2</sub>O was only decomposed as temperatures in excess of 300 °C (Fig. 5a).

With the assistance of CO, N<sub>2</sub> yields for both NO and N<sub>2</sub>O transformations were significantly improved up to 80% in NO + CO reaction and 91% in N<sub>2</sub>O + CO reaction even at 350 °C. Chien [41] et al. observed a higher NO adsorption rate for activated (reduced) than for unactivated LaCoO<sub>3</sub> and La<sub>0.85</sub>Ba<sub>0.15</sub>CoO<sub>3</sub>. A reduced perovskite surface with a large amount of anion vacancies was reported to be crucial for the NO dissociation according to FTIR and EPR spectroscopic analyses [8]. The role of CO seems therefore to maintain a reduced surface, which is necessary for successive NO dissociation. CO oxidation is also promoted by the O atom coming from NO or N<sub>2</sub>O (Fig. 5b). From the above results it seems that these tested perovskites act as “oxygen reservoir” transferring oxygen atoms from nitrogen oxides to CO thus achieving NO reduction and CO

oxidation simultaneously due to their outstanding redox properties.

The high reactivity of nitrosyl species toward CO was established via TPSR of NO under CO/He flow test. N<sub>2</sub>O formation was observed with a maximum of 346 ppm at 300 °C and further decreased at higher temperature (Fig. 4b). Based on our previous studies and present work, the catalytic mechanism (including the adsorption and transformation of reactants over perovskite, redox catalytic recycle, and the product components dependence on reaction temperature) is proposed to involve the following steps:

At low temperature, the dissociation of adsorbed NO species occurring over reduced perovskite and yielding N<sub>2</sub>O and N<sub>2</sub> was recognized as the rate determining step for catalytic reduction of NO by CO. The dimeric species of NO, such as N<sub>2</sub>O<sub>2</sub>, can be an intermediate, the formation of which involves the N–N bond formation and N–O bond cleavage [47,48]. Two parallel reactions for chemisorbed NO dissociation occurring over a reduced surface with N<sub>2</sub>O and N<sub>2</sub> as the respective products were assumed:



Reaction (14) involves the breakage of one N–O bond making this reaction much easier than reaction (13) which results in two N–O bond cleavages. This assumption is in agreement with the activity results shown in Fig. 4b, indicating that reaction (14) is dominating at low temperature. CO can be oxidized by M<sup>n+</sup>O<sup>−</sup> species as illustrated in Eq. (10) together with regeneration of anion vacancies on the surface for a continuous NO dissociation.

The reaction routes occurring at low temperature can thus be described as two parallel reactions:



Although N<sub>2</sub>O was detected in the effluent at low temperature (see Fig. 4b), its further conversion as an intermediate is not excluded [8,49,50]. Pomonis proposed a partially successive N<sub>2</sub>O decomposition (Route (3): 2N<sub>2</sub>O → 2N<sub>2</sub> + O<sub>2</sub>) occurring at low temperature simultaneously with reaction (16) over La<sub>1-x</sub>Sr<sub>x</sub>FeO<sub>3</sub> [7,51,52] and LaMnO<sub>3</sub> [52]. However, the N<sub>2</sub>O decomposition over the present perovskite was found to be quite difficult at T < 300 °C (see line for N<sub>2</sub>O decomposition in Fig. 5a) and is rather believed to occur only over a reduced perovskite with the participation of CO to consume surface oxygen species.

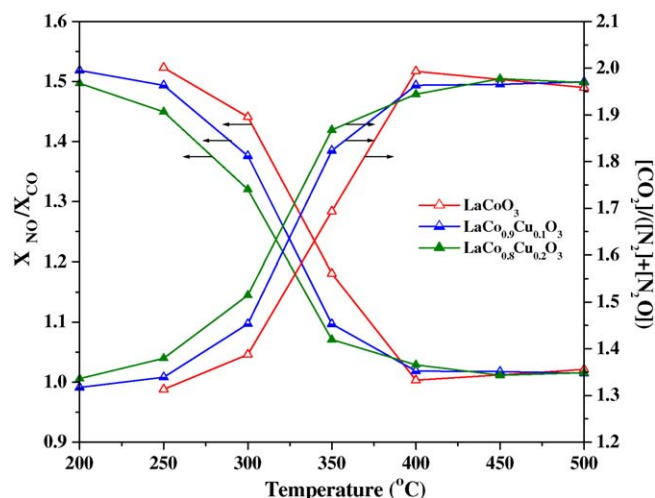
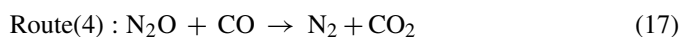


Fig. 7. Molar ratios of  $X_{\text{NO}}/X_{\text{CO}}$  and  $[\text{CO}_2]/([\text{N}_2] + [\text{N}_2\text{O}])$  in CO + NO reaction over Co-based perovskites, conditions: GHSV = 50,000 h<sup>-1</sup>, 3000 ppm NO, 3000 ppm CO, balanced by He.

The ratio of NO conversion to CO conversion must be equal to unity for Route (1) and two for Route (2), while the molar ratio  $\text{CO}_2/(\text{N}_2 + \text{N}_2\text{O})$  in the products should be two for Route (1) and one for Route (2) according to Eqs. (15) and (16). Therefore, the plots of  $X_{\text{NO}}/X_{\text{CO}}$  as well as  $[\text{CO}_2]/([\text{N}_2] + [\text{N}_2\text{O}])$  versus temperature provide an easy way to probe the reaction route involved. The  $X_{\text{NO}}/X_{\text{CO}}$  values were found to be close to 1.5 at  $T = 200$  °C and 1 at  $T > 400$  °C for lanthanum cobaltites. Moreover, the ratios of  $[\text{CO}_2]/([\text{N}_2] + [\text{N}_2\text{O}])$  for these catalysts are close to 1.3 at  $T = 200$  °C and 2 at  $T > 400$  °C as depicted in Fig. 7.

The reaction between CO and N<sub>2</sub>O (Route (4)) as well as the decomposition of N<sub>2</sub>O (Route (3)) are accelerated by rising temperature as depicted in Fig. 5a. As a result, all N<sub>2</sub>O generated during NO dissociation can be rapidly consumed and the reaction occurring at high temperature can be simplified as Route (1) with  $X_{\text{NO}}/X_{\text{CO}} = 1$  and  $[\text{CO}_2]/([\text{N}_2] + [\text{N}_2\text{O}]) = 2$ .

The kinetic analysis may be interpreted as another evidence supporting a mechanism dominated by Route (2) at low temperature and then gradually progressing into Route (1) at elevated temperature.

The higher conversion to N<sub>2</sub> obtained over LaCoO<sub>3</sub> compared to LaMnO<sub>3</sub> despite its lower surface area (Table 1) was ascribed to its higher surface density of anion vacancies (Table 2), which facilitates the adsorption of reactants (Tables 3 and 4) and further dissociation of chemisorbed NO (reactions (13) and (14)). Consequently, a significant improvement in N<sub>2</sub> yield was achieved after Cu incorporation into the B-sites of lanthanum cobaltite. Besides the essential effect of copper ions in the transformation of nitrogen oxides [12], Cu substitution can promote the formation of anion vacancies. At the same time, the regeneration of anion vacancies (see reaction (11)) is also accelerated after Cu substitution due to the enhancement in the mobility of lattice oxygen.

The overstoichiometric (excess) oxygen present in lanthanum manganite is also believed to participate in the oxidation of CO but without the generation of any oxygen vacancies, so that the

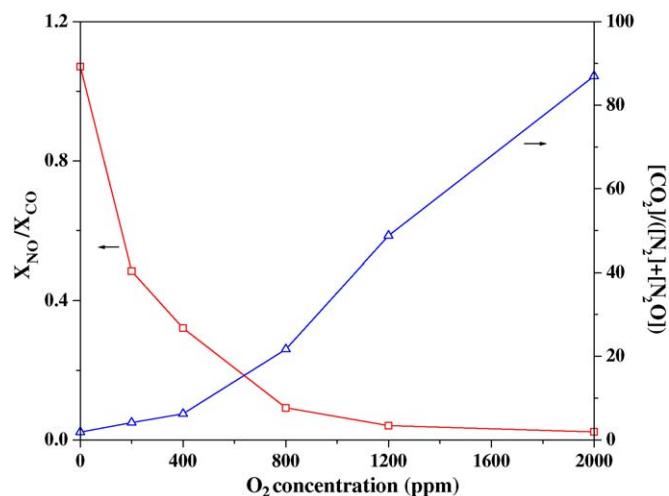


Fig. 8. Effect of O<sub>2</sub> feed concentration on the molar ratios of X<sub>NO</sub>/X<sub>CO</sub> and [CO<sub>2</sub>]/([N<sub>2</sub>] + [N<sub>2</sub>O]) in CO + NO reaction over LaCo<sub>0.8</sub>Cu<sub>0.2</sub>O<sub>3</sub>, conditions: GHSV = 50,000 h<sup>-1</sup>, T = 350 °C, 3000 ppm NO, 3000 ppm CO, 0–2000 ppm O<sub>2</sub>, balanced by He.

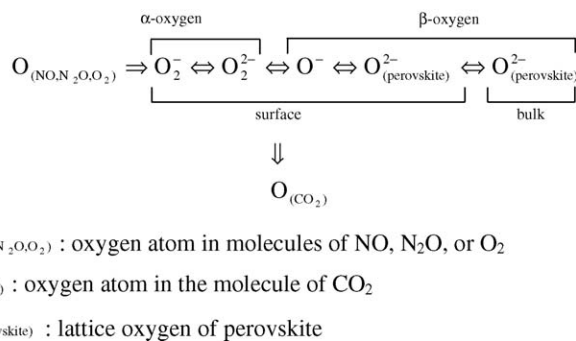
oxygen vacancies abundant in cobalt lanthanate seem to make a main contribution in NO + CO reaction compared with the overstoichiometric oxygen of manganese lanthanate.

#### 4.6. Effect of O<sub>2</sub> feed concentration on the catalytic behavior of LaCo<sub>0.8</sub>Cu<sub>0.2</sub>O<sub>3</sub>

A serious inhibiting effect of O<sub>2</sub> was observed in Fig. 6 during the reaction of 3000 ppm NO and 3000 ppm CO at 350 °C over LaCo<sub>0.8</sub>Cu<sub>0.2</sub>O<sub>3</sub>. The corresponding ratios of X<sub>NO</sub>/X<sub>CO</sub> and [CO<sub>2</sub>]/([N<sub>2</sub>] + [N<sub>2</sub>O]) as a function of O<sub>2</sub> feed concentration are plotted in Fig. 8, showing that X<sub>NO</sub>/X<sub>CO</sub> values diminish rapidly upon increasing O<sub>2</sub> concentration with values much lower than those for route (1) and route (2) at O<sub>2</sub> partial pressure above 800 ppm. The detrimental effect of oxygen became pronounced at O<sub>2</sub> concentration above 800 ppm, reflecting the fact that the reaction was totally controlled by the unfavorable oxidation of the reducing agent (Eq. (12)) leading to a far higher CO conversion compared to NO conversion. NO<sub>2</sub> is the main N-containing product under these conditions.

#### 4.7. The oxygen transfer in NO catalytic reduction by CO process

The interconversion of gaseous NO and CO due to homogeneous reaction is essentially negligible under usual reaction conditions, whereas a good catalytic performance in NO + CO reaction was achieved by catalysts, suggesting that oxygen transfer between NO and CO seems to occur indirectly and involves a catalytic process realized via perovskites. All of the atomic oxygens in perovskites, NO, N<sub>2</sub>O, and O<sub>2</sub> can be used for CO oxidation (Fig. 5b). The oxygen species (α-, and/or overstoichiometric, and β-oxygens) of Co- and Mn-based perovskites were also investigated by O<sub>2</sub>-TPD experiments (Fig. 1) and described in the discussion part of this paper. Based on the catalytic mechanism proposed here, the generation of oxygen vacancies is the



Scheme 1. Oxygen transformation behavior in the process of NO catalytic reduction by CO.

key process for a better activity in NO reduction. These anion vacancies can capture the oxygen atom from nitrogen oxides (NO or N<sub>2</sub>O) during NO dissociation to form surface lattice O<sup>-</sup>. The formation of α-oxygen (O<sub>2</sub><sup>-</sup>), which can further convert into adsorbed O<sub>2</sub><sup>2-</sup> or O<sup>-</sup> after getting one electron [48,53], likely takes place over perovskite when the reducing agent (CO) is insufficient in feed. Both α-oxygen and surface lattice O<sup>-</sup> may participate in the CO oxidation producing CO<sub>2</sub> and oxygen vacancies recovery for subsequent NO dissociation. Our previous studies of oxygen mobility in LaCoO<sub>3</sub> perovskites [53,54] showed that the adsorbed O<sub>2</sub> could exchange with the surface, and the exchanged atom could diffuse into the grain boundaries and into the bulk of the solid. Oxygen transfer in NO catalytic reduction by CO is illustrated as Scheme 1: the transfer of oxygen from NO to CO involving the generation of surface lattice oxygen atoms due to NO dissociation (Eqs. (8), (13) and (14)), and reduction of surface lattice O<sup>-</sup> into oxygen vacancies by CO (Eq. (10)). The high catalytic activity (especially at low temperature) achieved over lanthanum cobaltite was ascribed to its large density of surface oxygen vacancies providing more active sites for reactant adsorption and reaction. Cu substitution further promotes the catalytic performance through not only increasing oxygen vacancies but also enhancing the lattice oxygen mobility.

## 5. Conclusion

Nanocrystalline perovskite-type oxides were prepared by reactive grinding with specific surface areas of 20–30 m<sup>2</sup>/g for Co-based perovskites and approximately 40 m<sup>2</sup>/g for Mn-based perovskites, even after calcination at 500 °C for 5 h. The somewhat porous structure of these materials was achieved via clustering of individual primary particles.

A broad α-O<sub>2</sub> desorption was observed during O<sub>2</sub>-TPD for lanthanum cobaltite, indicating the abundance of oxygen vacancies present over the surface of this perovskite. More oxygen vacancies were generated after partial substitution by Cu<sup>2+</sup> due to a positive charge deficiency. These anion vacancies seem to play an important role in catalytic reduction of NO providing the adsorption sites for NO and CO as well as promoting the dissociation of adsorbed NO species. In contrast, a significant desorption of overstoichiometric oxygen from lanthanum manganite was found, which was suppressed by Cu incorporation into lattice B-sites. The role of this excess oxygen seems to just

accelerate the oxidation of the reducing agent, with less contribution in NO reduction since no anion vacancies are generated during CO oxidation by this overstoichiometric oxygen.

Cu partial substitution can also enhance not only the abundance of anion vacancies but also the mobility of lattice oxygen in lanthanates to accelerate the oxidation of CO by surface lattice oxygen with regeneration of the anion vacancies. Accordingly, a significant improvement in catalytic performance of NO + CO reaction was achieved by introduction of Cu ions into the B-sites of perovskites.

At low temperature, the chemisorbed NO (nitrosyl species) was dissociated over perovskites with the formation of both N<sub>2</sub> and N<sub>2</sub>O as well as an oxidized surface. The oxidized surface can be reduced by CO in these conditions with regeneration of anion vacancies for the continuous reaction. N<sub>2</sub>O was further reduced by CO and this transformation becomes more significant as temperature increases.

NO decomposition is difficult over LaCo<sub>0.8</sub>Cu<sub>0.2</sub>O<sub>3</sub> as temperature below 500 °C. In contrast, N<sub>2</sub>O can be decomposed at  $T > 300$  °C, achieving a N<sub>2</sub> yield of 68% at 500 °C and 50,000 h<sup>-1</sup> GHSV. Nevertheless, both NO and N<sub>2</sub>O transformations are obviously promoted in the presence of CO.

O<sub>2</sub> strongly inhibits N<sub>2</sub> yield by suppressing the reducing agent through complete CO oxidation. As a result the total NO + CO reaction in the presence of O<sub>2</sub> was found to be severely limited by CO oxidation.

In previous works [15,16] we have studied the catalytic reduction of NO by propylene over the same catalysts. In these studies we have found that the main NO reduction process involved surface nitrate species NO<sub>3</sub><sup>-</sup>. This is in contrast with the conclusions of the present work, which considers the nitrosyl species NO<sup>-</sup> as the main adsorbed reactant (Eqs. (13) and (14)). The difference between the two systems is due to the higher efficiency of CO (compared to propene) in reducing the perovskite surface (Eqs. (10)–(12)).

In the presence of propene and oxygen in the gas phase, the surface concentration of O<sub>2</sub><sup>-</sup> species is higher (compared to CO alone) and therefore the NO<sub>3</sub><sup>-</sup> surface density is also higher. It is this species, which is then reduced by propene. The nitrosyl species are in lower concentration (again compared to CO in the gas phase) and do not react with propene.

Thus the NO catalytic reduction is entirely different with these two reducing agents.

## Acknowledgements

The financial support of NSERC through its industrial chair program is gratefully acknowledged. We thank Nanox Inc. for the preparation of the perovskite samples.

## References

- [1] W.P.A. Jansen, J.M.A. Harmsen, A.W.D.v.d. Gon, J.H.B.J. Hoebink, J.C. Schouten, H.H. Brongersma, *J. Catal.* 204 (2001) 420–427.
- [2] H.S. Gandhi, G.W. Graham, R.W. McCabe, *J. Catal.* 216 (2003) 433–442.
- [3] G. Parravano, *J. Chem. Phys.* 20 (1952) 342–343.
- [4] W.F. Libby, *Science* 171 (1971) 499–500.
- [5] L. Lisi, G. Bagnasco, P. Ciambelli, S.D. Rossi, P. Porta, G. Russo, M. Turco, *J. Solid State Chem.* 146 (1999) 176–183.
- [6] V.C. Belessi, C.N. Costa, T.V. Bakas, T. Anastasiadou, P.J. Pomonis, A.M. Efstathiou, *Catal. Today* 59 (2000) 347–363.
- [7] A.A. Leontiou, A.K. Ladavos, P.J. Pomonis, *Appl. Catal. A: Gen.* 241 (2003) 133–141.
- [8] L. Forni, C. Oliva, T. Barzetti, E. Selli, A.M. Ezerets, A.V. Vishniakov, *Appl. Catal. B: Environ.* 13 (1997) 35–43.
- [9] V.C. Belessi, T.V. Bakas, C.N. Costa, A.M. Efstathiou, P.J. Pomonis, *Appl. Catal. B: Environ.* 28 (2000) 13–28.
- [10] A.A. Leontiou, A.K. Ladavos, G.S. Armatas, P.N. Trikalitis, P.J. Pomonis, *Appl. Catal. A: Gen.* 263 (2004) 227–239.
- [11] S.D. Peter, E. Garbowski, V. Perrichon, B. Pommier, M. Primet, *Appl. Catal. A: Gen.* 205 (2001) 147–158.
- [12] G. Centi, S. Perathoner, *Appl. Catal. A: Gen.* 132 (1995) 179–259.
- [13] H. Yahiro, M. Iwamoto, *Appl. Catal. A: Gen.* 222 (2001) 163–181.
- [14] Y. Wan, J.X. Ma, Z. Wang, W. Zhou, S. Kaliaguine, *J. Catal.* 227 (2004) 242–252.
- [15] R.D. Zhang, A. Villanueva, H. Alamdari, S. Kaliaguine, *Appl. Catal. B: Environ.* 64 (2006) 220–233.
- [16] R.D. Zhang, A. Villanueva, H. Alamdari, S. Kaliaguine, *Appl. Catal. A: Gen.* 307 (2006) 85.
- [17] R.D. Zhang, A. Villanueva, H. Alamdari, S. Kaliaguine, *J. Catal.* 237 (2006) 368–380.
- [18] M. Crespin, W.K. Hall, *J. Catal.* 69 (1981) 359–370.
- [19] A.E. Giannakas, T.C. Vaimakis, A.K. Ladavos, P.N. Trikalitis, P.J. Pomonis, *J. Colloid Interface Sci.* 259 (2003) 244–253.
- [20] X. Li, H.B. Zhang, X.X. Liu, S.J. Li, M.Y. Zhao, *Mater. Chem. Phys.* 38 (1994) 355–362.
- [21] C. Xiulan, L. Yuan, *Chem. Eng. J.* 78 (2001) 205–209.
- [22] G. Sinquin, C. Petit, J.P. Hindermann, A. Kiennemann, *Catal. Today* 70 (2001) 183–196.
- [23] R.J.H. Voorhoeve, D.W. Johnson Jr., J.P. Remeika, P.K. Gallagher, *Science* 195 (1977) 827–833.
- [24] J. Kirchnerova, D. Klvana, *Int. J. Hydrogen Energy* 19 (1994) 501–506.
- [25] R. Leanza, I. Rossetti, L. Fabbri, C. Oliva, L. Forni, *Appl. Catal. B: Environ.* 28 (2000) 55–64.
- [26] S. Kaliaguine, A. van Neste, (Process For Synthesizing Perovskites Using High Energy Milling, USA), US Patent US 6017504 (2000) 10 pp.
- [27] S. Kaliaguine, A. van Neste, V. Szabo, J.E. Gallot, M. Bassir, R. Muzychuk, *Appl. Catal. A: Gen.* 209 (2001) 345–358.
- [28] V. Szabo, M. Bassir, A. Van Neste, S. Kaliaguine, *Appl. Catal. B: Environ.* 43 (2003) 81–92.
- [29] S. Royer, A. van Neste, R. Davidson, S. McIntyre, S. Kaliaguine, *Ind. Eng. Chem. Res.* 43 (2004) 5670–5680.
- [30] P. Porta, S.D. Rossi, M. Faticanti, G. Minelli, I. Pettiti, L. Lisi, M. Turco, *J. Solid State Chem.* 146 (1999) 291–304.
- [31] J.A.M. van Roosmalen, E.H.P. Cordfunke, R.B. Helmholtz, H.W. Zandbergen, *J. Solid State Chem.* 110 (1994) 100–105.
- [32] L.A. Isupova, A.A. Budneva, E.A. Paukshtis, V.A. Sadykov, *J. Mol. Catal. A: Chem.* 158 (2000) 275–280.
- [33] G. Centi, *Mater. Eng.* 5 (1994) 79–85.
- [34] X. She, M. Flytzani-Stephanopoulos, *J. Catal.* 237 (2006) 79–93.
- [35] B. Coq, D. Tachon, F. Figueras, G. Mabilon, M. Prigent, *Appl. Catal. B: Environ.* 6 (1995) 271–289.
- [36] S. Shin, H. Arakawa, Y. Hatakeyama, K. Ogawa, K. Shimomura, *Mater. Res. Bull.* 14 (1979) 633–639.
- [37] V.A. Matyshak, O.V. Krylov, *Catal. Today* 25 (1995) 1–87.
- [38] J.M.D. Tascón, L.G. Tejuca, C.H. Rochester, *J. Catal.* 95 (1985) 558–566.
- [39] R.J.H. Voorhoeve, *Advanced Materials in Catalysis*, New York, 1977, p. 129.
- [40] B. Viswanathan, *Catal. Rev. -Sci. Eng.* 34 (4) (1992) 337–354.
- [41] M.W. Chien, I.M. Pearson, K. Nobe, *Ind. Eng. Chem., Prod. Res. Dev.* 14 (1975) 131–134.
- [42] C. Shi, M. Cheng, Z. Qu, X. Yang, X. Bao, *Appl. Catal. B: Environ.* 36 (2002) 173–182.
- [43] V.I. Pârvulescu, P. Grange, B. Delmon, *Catal. Today* 46 (1998) 233–316.

- [44] Y. Teraoka, H. Fukuda, S. Kagawa, *Chem. Lett.* (1990) 1–4.
- [45] H. Yasuda, N. Mizuno, M. Misono, *J. Chem. Soc., Chem. Commun.* (1990) 1094–1096.
- [46] C. Tofan, D. Klvana, J. Kirchnerova, *Appl. Catal. A: Gen.* 223 (2002) 275–286.
- [47] J. Valyon, W.K. Hall, *J. Phys. Chem.* 97 (1993) 1204–1212.
- [48] H.X. Dai, H. He, P.H. Li, Zh.L. Gao, C.-T. Au, *Catal. Today* 90 (2004) 231–244.
- [49] L.G. Tejuca, J.L.G. Fierro, J.M.D. Tascón, *Adv. Catal.* 36 (1989) 237–327.
- [50] P.J. Gellings, H.J.M. Bouwmeester, *Catal. Today* 12 (1992) 1–101.
- [51] V.C. Belessi, P.N. Trikalitis, A.K. Ladavos, T.V. Bakas, P.J. Pomonis, *Appl. Catal. A: Gen.* 177 (1999) 53–68.
- [52] A.E. Giannakas, A.K. Ladavos, P.J. Pomonis, *Appl. Catal. B: Environ.* 49 (2004) 147–158.
- [53] S. Royer, D. Duprez, S. Kaliaguine, *Catal. Today* 112 (2006) 99–102.
- [54] S. Royer, D. Duprez, S. Kaliaguine, *J. Catal.* 234 (2005) 364–375.